

Interplay of magnetic and hydrogen ordering in the hexagonal Laves hydrides

O. L. Makarova,¹ I. N. Goncharenko,^{1,2,*} A. V. Irodova,¹ I. Mirebeau,² and E. Suard³

¹Russian Research Center "Kurchatov Institut," 123182 Moscow, Russia

²Laboratoire Léon Brillouin, CEA-CNRS, CEA/Saclay, 91191 Gif sur Yvette, France

³Institut Laüe Langevin, 156X, 38042 Grenoble, France

(Received 3 April 2002; published 25 September 2002)

We have studied the magnetic and crystal structures of the hexagonal Laves phases RMn_2H_x ($R = \text{Er, Tm, Lu}$; $x = 4.2, 4.6$) by powder neutron diffraction. Hydrogen occupies interstitial sites of the metal lattice and forms ordered superstructures. Hydrogen stabilizes localized magnetic moments on the Mn sites by expanding the metal lattice. We have found a very strong coupling between the magnetic and structural properties of the hydrides. Very small modifications in the hydrogen sublattice result in drastic changes in the magnetic properties. The samples $RMn_2H_{4.6}$ show a long-range antiferromagnetic ordering (propagation vector $\mathbf{k} = 1/3 \ 1/3 \ 0$), whereas the samples $RMn_2H_{4.2}$ exhibit short-range magnetic correlations. We discuss our results in the framework of a model assuming that the magnetic ordering is driven by hydrogen superstructure which changes the local symmetries of the magnetic ions and releases the topological frustration in the Mn sublattice.

DOI: 10.1103/PhysRevB.66.104423

PACS number(s): 75.25.+z, 75.50.Ee, 61.12.Ld

I. INTRODUCTION

The Laves phases RMn_2 ($R = \text{rare earth}$) have been intensively studied because of their unusual structural and magnetic properties. These compounds have two magnetic sublattices: the first one is formed by well-localized $4f$ magnetic moments of the rare earth, whereas the second one is formed by unstable $3d$ magnetic moments of the Mn atoms. The $3d$ shells are close to the instability limit between localized and itinerant states and lose their intrinsic magnetic moments when first-neighbor Mn-Mn distance d becomes smaller than some critical distance $d_c \sim 2.7 \text{ \AA}$. Consequently, the RMn_2 compounds can be divided into three groups.

(I) $d < d_c$ ($\text{LuMn}_2, \text{ErMn}_2, \text{TmMn}_2$). The Mn sublattice is nonmagnetic. The compounds are nonmagnetic (LuMn_2) or ferromagnetic if $R = \text{magnetic rare earth}$ (ErMn_2 and TmMn_2).¹

(II) $d > d_c$ ($\text{NdMn}_2, \text{PrMn}_2$). The Mn atoms carry stable magnetic moments. The Mn magnetism dominates and imposes an antiferromagnetic ordering in the rare-earth sublattice through the R -Mn magnetic exchange.²

(III) $d \sim d_c$ ($\text{GdMn}_2, \text{TbMn}_2, \text{DyMn}_2, \text{HoMn}_2, \text{YMn}_2$). Mn moments are very close to the instability limit. In DyMn_2 and TbMn_2 the exchange field of the rare-earth moments induces magnetic moments in the Mn sublattice. This group is characterized by complicated noncollinear magnetic ordering and/or by the coexistence of magnetic and nonmagnetic Mn sites.³⁻⁶

Another important feature of the RMn_2 compounds arises from the topological properties of the Mn sublattice. The RMn_2 ($R = \text{Y}$ or rare earth) compounds crystallize in the cubic $C15$ ($R = \text{Gd, Tb, Dy, Ho}$) or hexagonal $C14$ ($R = \text{Pr, Nd, Sm, Er, Tm, Lu}$) structures. In both structures the Mn sublattice is formed by regular Mn_4 tetrahedra. In the hexagonal structure the tetrahedra form chains along the c axis, whereas in the cubic structure the tetrahedra form a corner-sharing three-dimensional lattice. In another way, the Mn sublattices in both cubic and hexagonal phases could be de-

scribed as a stacking of simple triangular planes and *kagomé*-like planes either along the c axis ($C14$ structure) or along the cubic diagonal ($C15$ structure). Below, we will call Mn(1) the atoms belonging to the simple triangular planes and Mn(2) the atoms belonging to the *kagomé* planes. The *kagomé* planes are considerably denser than the triangular ones. The first-neighbor distances between the Mn(2) atoms are $1/\sqrt{3}$ times the first-neighbor distances between the Mn(1) atoms.

In both cases ($C14$ or $C15$) the first-neighbor antiferromagnetic interactions result in a fully degenerated magnetic ground state. The topological frustration could be released by a structural distortion (YMn_2) (Refs. 6 and 7) or by the suppression of magnetic moments on some magnetic sites (ThMn_2).⁸ The combined effect of topological frustration and instability of magnetic moments in the RMn_2 Laves compounds results in very peculiar magnetic properties (giant spin fluctuations, spin-liquid ground state, complicated magnetic ordering, etc.), which have been intensively studied during the last two decades.

The RMn_2 compounds can absorb large quantities of hydrogen (up to 4–4.6 per formula unit). Interstitial hydrogen leads to significant changes of the magnetic and structural properties. Hydrogen occupies interstitial sites of the metal host and expands the lattice. The lattice expansion can stabilize magnetic moments on the Mn sites. Moreover, hydrogen atoms form ordered superstructures and release frustration by changing the local environment of the Mn atoms. The effect of hydrogen absorption on the magnetic properties of $C15$ cubic RMn_2 compounds has been studied by different techniques.⁹⁻¹¹ Recently, a systematic study of $RMn_2H_{4.3}$ hydrides ($R = \text{Y, Gd, Tb, Dy, Ho}$) revealed a very intricate coupling between magnetic and structural ordering. Magnetic and hydrogen superstructures have the same symmetry and appear at the same temperature through a first-order magnetostructural transition.^{12,13} This very intricate behavior was explained by a model assuming that hydrogen influences the magnetic ordering by releasing topological frustration in the Mn sublattice.

Very little is known about the structural and magnetic properties of the *C14* hexagonal hydrides RMn_2H_x ($R = \text{Er, Tm, Lu}$). These compounds absorb hydrogen up to 4.6 atoms per formula unit. The nonmonotonic lattice expansion upon hydrogenation suggests the presence of (at least) two different phases with hydrogen contents $x = 4 - 4.2$ and $x = 4.5 - 4.6$.¹⁴ However, nothing is known about the location of hydrogen atoms in these phases and about the possible physical reasons for the existence of two separate phases having very close hydrogen contents. It was suggested that interstitial hydrogen strongly influences the magnetic properties of the *C14* phases. Magnetization measurements of LuMn_2H_x (hydrogen content was not defined, but expected to be close to the maximal one) suggested a transition from a paramagnetic to a ferromagnetic state below 200 K.¹⁵ In contrast, ¹⁶⁶Er Mössbauer measurements did not show any evidence for a magnetic ordering in $\text{ErMn}_2H_{4.6}$ at $T = 4$ K and a paramagnetic state of the rare-earth sublattice had been claimed.¹⁴

Neutron diffraction is the most suitable tool to study both hydrogen and magnetic ordering, since neutrons are well scattered by light elements and by magnetic moments. Here we present a systematic neutron diffraction study of the hexagonal hydrides $RMn_2H_{4.2}$ and $RMn_2H_{4.6}$ ($R = \text{Er, Tm, Lu}$). We refined the magnetic and crystal structures and searched for a possible interplay between magnetic and structural ordering.

II. EXPERIMENTAL DETAILS

The starting intermetallic compounds have been prepared by arc melting from Mn of 99.99% purity and rare-earth metals of 99.9% purity. In most cases, we used the deuterium isotope in order to decrease the incoherent scattering in neutron experiments. Below, we will speak of hydrogen and deuterium indifferently. The hydrides were prepared by absorption of deuterium gas at the pressure 0.4–0.7 bar. The hydrogen content was estimated by measuring the volume of the absorbed gas. By choosing an appropriate temperature for the synthesis ($T = 273$ and 140 K) we prepared samples with different hydrogen concentrations ($x = 4.2$ and 4.6, respectively). The samples were exposed to hydrogen until equilibrium was attained.

The sample quality and symmetry of the metal lattice were checked by x-ray diffraction at ambient temperature. All the samples retain the hexagonal symmetry of the unit cell. The c/a ratios ($c/a = 1.66$ and 1.64 for $x = 4.2$ and 4.6, respectively) in the hydrides are slightly larger than in the parent compounds ($c/a = 1.63$). The hydrogen absorption results in an increase of the lattice constants. The unit-cell volumes of the $RMn_2H_{4.2}$ compounds are about 25% higher than in the parent compounds. In the concentration range $0 < x < 4.2$ the volume increases almost linearly with the hydrogen content. Adding an additional 0.4 atoms per formula unit results in an anomalous expansion of the unit cell, $\Delta V/V = 7.5\%$. This value is about 3 times larger than the value obtained by extrapolating the volume dependence $V(x)$ measured in the concentration range $0 < x < 4.2$. All samples with hydrogen contents between $x = 4.2$ and 4.6

were mixtures of the low-content ($x = 4.2$) and high-content ($x = 4.6$) phases. Even samples with the highest hydrogen concentration allowed by synthesis ($x = 4.6 - 4.7$) contain small amounts of the low-content phase ($x = 4.2$). The amount increases (5% in $\text{ErMn}_2H_{4.6}$ and $\text{TmMn}_2H_{4.6}$ and 25% in $\text{LuMn}_2H_{4.6}$) as the ionic radius of the rare earth decreases. In order to obtain a single-phase hydride with nonmagnetic *R* sublattice and hydrogen content $x = 4.6$ we used a partial Lu/Y substitution, which expands the unit cell while keeping the *C14* structure. The sample $(\text{Lu}_{0.4}\text{Y}_{0.6})\text{Mn}_2H_{4.6}$ has a hexagonal (*C14*) structure and less than 5% of the low-content phase.

Neutron diffraction experiments were performed on the high-resolution diffractometer D2B at the Institut Laue Langevin (incident neutron wavelength 1.59 Å) and on the high-intensity diffractometer G6.1 at the Laboratoire Léon Brillouin (incident neutron wavelength 4.74 Å). Both magnetic and crystal structures were analyzed using the FULLPROF program based on the Rietveld method.¹⁶

III. CRYSTAL STRUCTURE

A. $RMn_2H_{4.2}$

In the Laves structures, hydrogen atoms may occupy the $2R + 2Mn$, $R + 3Mn$, and $4Mn$ interstitial sites in the metal lattice. By analogy with the cubic RMn_2H_x compounds we expected that the hydrogen would preferably occupy the $2R + 2Mn$ sites.

The neutron diffraction patterns of the low-content samples $\text{ErMn}_2H_{4.2}$ are shown in Fig. 1. Diffraction patterns measured at $T = 300$ K do not show any additional peaks with respect to the space group $P6_3/mmc$ which could be associated with a hydrogen superstructure. A broad diffuse peak around $2\theta = 45^\circ$ is attributed to short-range liquidlike correlation in the disordered hydrogen sublattice. Analyzing the neutron diffraction data assuming a fully random distribution of 16.8 hydrogen atoms among the 48 $2R + 2Mn$ interstitial sites of the unit cell containing 4 formula units yielded a good agreement between the calculated and experimental profiles ($R_p < 5\%$).

Below $T = 300$ K we observed additional reflections (hhl type where l is odd) forbidden in the space group $P6_3/mmc$. They could be seen in the inset of Fig. 1. In the same temperature range the intensity of the diffuse peak at $2\theta = 45^\circ$ decreases. The appearance of the superstructural peaks and the decrease of the diffuse scattering suggest the formation of hydrogen ordering. We searched for all possible variants of hydrogen ordering in the $2R + 2Mn$ interstitial sites satisfying the following criteria: (i) hexagonal symmetry of the unit cell (i.e., the lowest possible symmetry is $P3$), (ii) number of allowed hydrogen positions more than 16.8 per unit cell containing 4 formula units, and (iii) the shortest H-H distance $d_{\text{H-H}} > 2.1$ Å (so-called “blocking” condition¹⁷).

We found only one model (shown in Fig. 2) providing a reasonable agreement ($R_p < 10\%$) with the experimental data for the compounds $RMn_2H_{4.2}$. The best refinement ($R_p = 5\%$) was obtained assuming a partial hydrogen disorder

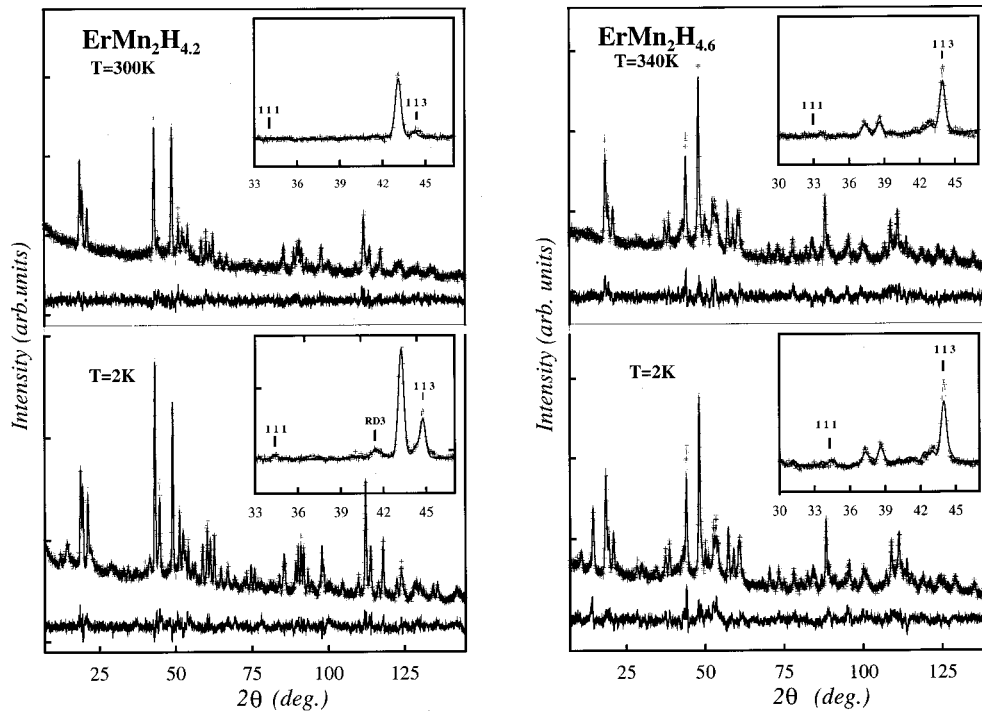


FIG. 1. Observed, calculated, and difference neutron diffraction patterns of $\text{ErMn}_2\text{H}_{4.2}$ and $\text{ErMn}_2\text{H}_{4.6}$ measured at D2B ($\lambda = 1.59 \text{ \AA}$). Insets: superstructural peaks forbidden in the space group $P6_3/mmc$.

among the $6h$ positions. The space group is $P6_3/m$. The parameters of the crystal structure $\text{RMn}_2\text{H}_{4.2}$ are given in Table I.

B. $\text{RMn}_2\text{H}_{4.6}$

In contrast with the low-content phase, in the $\text{RMn}_2\text{H}_{4.6}$ the superstructural peaks (hkl type) persist up to the highest measured temperature 340 K (see inset of Fig. 1). The intensities of the superstructural peaks are almost temperature independent. We did not observe any significant diffuse scattering which could be associated with hydrogen disorder.

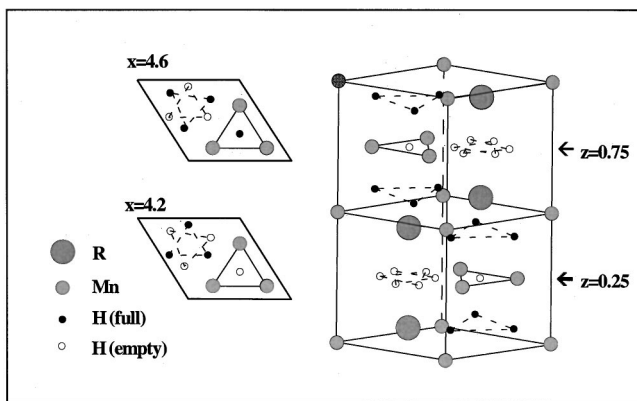


FIG. 2. Schematic drawing of the hydrogen superstructures in $\text{RMn}_2\text{H}_{4.6}$ and $\text{RMn}_2\text{H}_{4.2}$. Right: filling of the hydrogen positions between the Mn planes. These positions are occupied in the same way in the low-content ($x=4.2$) and high-content ($x=4.6$) hydrides. Left: position of hydrogen atoms inside of the Mn(2) *kagomé* planes in $\text{RMn}_2\text{H}_{4.6}$ (top) and $\text{RMn}_2\text{H}_{4.2}$ (bottom).

Above 340 K the hydrides are expected to decompose: therefore, we conclude that the hydrogen ordering persists in the whole temperature range up to the temperature of hydrogen desorption.

We used the same procedure as above to search for a possible hydrogen ordering. Since we did not observe any split of the structural peaks, we constrained the lowest possible symmetry to $P3$ (as we did for the low-content phases). Surprisingly, none of the possible hydrogen arrangements in the $2R+2\text{Mn}$ interstitial sites satisfying the $P3$ symmetry and the blocking conditions ($d_{\text{H-H}} > 2.1 \text{ \AA}$) gave a satisfactory agreement with the experimental data. Then we considered structural models involving other kinds of interstitial sites, namely $R+3\text{Mn}$ and 4Mn . We found a satisfactory model assuming that some hydrogens occupy the $R+3\text{Mn}$ sites. In this model, 17 hydrogen atoms (per unit cell) occupy $2R+2\text{Mn}$ sites in the same way as in the low-content phase, except the atoms located in the positions $6h$ and lying in the Mn(2) *kagomé* plane (see Fig. 2). The remaining hydrogen atoms (1.6 per unit cell) occupy one-quarter of the $R+3\text{Mn}$ sites (positions $4f$) with occupancy 0.4. Although the model qualitatively agrees with the experimental data, the fits have relatively large R factors ($R_p = 12\%$). The agreement could be improved by varying the positions of the hydrogen atoms inside the tetrahedra. H atoms located in the $R+3\text{Mn}$ sites were found displaced towards the base of the tetrahedra formed by three Mn atoms and lying in the Mn(2) plane. Each 3Mn triangle is shared by two neighboring $R+3\text{Mn}$ tetrahedra. Each pair of tetrahedra forms a $2R+3\text{Mn}$ bipyramide. In the best fit, the hydrogen atoms lie in the Mn(2) planes and occupy the centers of the $2R+3\text{Mn}$ bipyramids (positions $2d$, occupancy 0.8). This model gave

TABLE I. Crystal structural parameters of $\text{LuMn}_2\text{H}_{4.2}$ at $T=2$ K. Space group $P6_3/m$. Parameters given without error bars in brackets were not fitted.

Atom	Position	Occupancy	Position parameters			Static or temperature displacements (\AA^2)
			x	y	z	
Lu	$4f$	1.00	0.333	0.667	0.0625	0.2
Mn(1)	$2b$	1.00	0.000	0.000	0.000	0.4
Mn(2)	$6h$	1.00	-0.150(9)	-0.325(9)	0.250(0)	0.4
H ₁	$12i$	0.78(7)	0.052(6)	0.321(8)	0.571(5)	1.0(5)
H ₂	$12i$	0.05(4)	-0.321(8)	-0.052(6)	0.571(5)	1.0(5)
H ₃	$12i$	0.18(5)	0.560(4)	0.095(4)	0.145(5)	1.0(5)
H ₄	$6h$	0.74(2)	0.448(8)	0.934(9)	0.250(0)	1.0(5)
Deuterium atoms per formula unit			4.14			
Reliability factors (%)			$R_p=4.7\%$	$R_f=6.51\%$	$R_B=7.39\%$	
Lattice constants (\AA)			$a=5.571(4)$	$c=9.268(8)$		

a satisfactory agreement between the calculated and measured spectra ($R_p=5\%$). Filling the $2R+3\text{Mn}$ intersites yields a considerable volume expansion and significant displacements of the Mn atoms from their ideal positions. In the final model each Mn(2) plane hosts 3.8 hydrogen atoms per unit cell (3 in positions $2R+2\text{Mn}$ and 0.8 in positions $2R+3\text{Mn}$). Final parameters are given in Table II.

IV. MAGNETIC STRUCTURE

The magnetic neutron scattering in $\text{ErMn}_2\text{H}_{4.2}$ and $\text{ErMn}_2\text{H}_{4.6}$ measured at the high-wavelength diffractometer G6.1 is shown in Figs. 3 and 4 (left). In order to separate the magnetic contribution we subtracted spectra measured in paramagnetic range ($T>250$ K). The magnetic peaks could be easily distinguished from the superstructural peaks associated with hydrogen ordering by their insensitivity to isotopic H(D) substitution. We found very different magnetic behaviors in the low-content and high-content hydrides. In $\text{RMn}_2\text{H}_{4.6}$ we observed sharp magnetic peaks in the temperature range $T<250$ K. We do not observe any magnetic contribution to the structural peaks: therefore, we conclude that

the magnetic structure is purely antiferromagnetic. Narrow widths point out a long-range magnetic ordering. In contrast, the low-content samples $\text{RMn}_2\text{H}_{4.2}$ show no evidence of a long-range magnetic ordering. In these samples, we observed broad diffuse peaks associated with presence of short-range magnetic correlations.

In the long-range ordered hydrides $\text{RMn}_2\text{H}_{4.6}$ the magnetic peaks could be indexed by the propagation vector $\mathbf{k}=1/3\ 1/3\ 0$. Neither the propagation vector nor the ordering temperature depend on substitution in the R sublattice. The magnetic intensities and their temperature dependences show very little difference between the compounds with non magnetic ($R=\text{Lu}$ or mixture Lu, Y) and magnetic ($R=\text{Tm,Er}$) R sublattice. Below 100 K we observed only very small contributions from the magnetic R ($R=\text{Er,Tm}$) atoms to total magnetic scattering (Fig. 3, right).

The propagation vector $\mathbf{k}=1/3\ 1/3\ 0$ corresponds to a 120° rotation of the magnetic moments in the ab plane (see Fig. 5). A precise determination of the magnetic structure was performed using the Rietveld technique. Refining the individual values of the magnetic moments and their orientations for all magnetic atoms in the unit cell makes the

TABLE II. Crystal structural parameters of $(\text{Lu}_{0.4}\text{Y}_{0.6})\text{Mn}_2\text{D}_{4.6}$ at $T=2$ K. Space group $P6_3/m$. Parameters given without error bars in brackets were not fitted.

Atom	Position	Occupancy	Position parameters			Isotropic (B) or anisotropic (β) displacement parameters (\AA^2 and \AA , respectively)		
			x	y	z			
Lu, Y	$4f$	1.00	0.333	0.667	0.059(2)	$B=0.2$		
Mn(1)	$2b$	1.00	0.000	0.000	0.000	$B=0.6$		
Mn(2)	$6h$	1.00	-0.149(4)	-0.312(3)	0.250	$\beta_{11}=0.002(1)$	$\beta_{22}=0.008(2)$	$\beta_{33}=0.003(1)$
H ₁	$12i$	0.98(2)	0.052(7)	0.347(8)	0.572(8)	$\beta_{11}=0.010(1)$	$\beta_{22}=0.033(2)$	$\beta_{33}=0.004(1)$
H ₂	$6h$	0.90(1)	0.158(8)	0.403(9)	0.250	$\beta_{11}=0.006(2)$	$\beta_{22}=0.016(3)$	$\beta_{33}=0.006(2)$
H ₃	$2d$	0.78(3)	0.667(0)	0.333(0)	0.250	$\beta_{11}=0.000$	$\beta_{22}=0.000$	$\beta_{33}=0.049(1)$
Deuterium atoms per formula unit					4.68			
Reliability factor (%)					$R_p=5.24\%$	$R_{\text{expt}}=6.79\%$	$R_B=14.4\%$	
Lattice constant (\AA)					$a=5.789(2)$	$c=9.536(3)$		

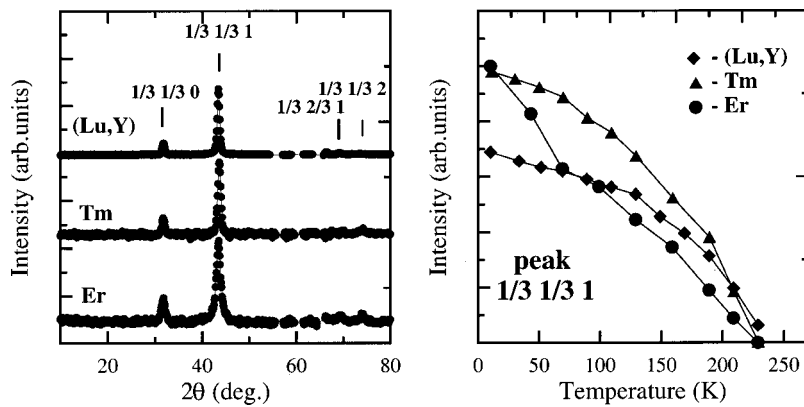


FIG. 3. Left: magnetic scattering in $RMn_2H_{4.6}$ measured on the long-wavelength diffractometer G6.1 ($\lambda = 4.74 \text{ \AA}$) at $T = 10 \text{ K}$. The spectra are subtracted from the neutron diffraction patterns measured in the paramagnetic range ($T = 280\text{--}290 \text{ K}$). Right: integrated intensities of the $1/3 \ 1/3 \ 1$ peak vs temperature. Solid lines are guides to the eye.

fitting procedure unstable. Therefore we constrained the values of $Mn(R)$ moments to be the same for all $Mn(R)$ sites and to be lying in the basal planes. We also constrained the angles between the directions of the magnetic moments in different ab planes to be equal to $2\pi/n$ ($n = 1, 2, 3, 4, 6$). The refined parameters for $ErMn_2H_{4.6}$ are given in Table III. Spin directions in $(Lu_{0.4}Y_{0.6})Mn_2H_{4.6}$ and $TmMn_2H_{4.6}$ are the same as in $ErMn_2H_{4.6}$. Values of ordered magnetic moments measured at different temperatures in all $RMn_2H_{4.6}$ compounds are shown in Fig. 6. The values of magnetic moments on the Mn sites ($\mu_{Mn} \approx 2.5 \mu_B$) are close to the values found in other RMn_2 compounds having well-localized Mn magnetic shells. The values of magnetic moments on the rare-earth sites are significantly lower than the free ion values: $\mu_{(R)} = 2.6 \mu_B$ for $ErMn_2H_{4.6}$ and $TmMn_2H_{4.6}$ instead of $9 \mu_B$ and $7 \mu_B$ for Er^{3+} and Tm^{3+} , respectively.

The above model gives reliability factors $R_{mag} = 14\%$, 17% , and 20% for $Lu_{0.4}Y_{0.6}Mn_2H_{4.6}$, $TmMn_2H_{4.6}$, and $ErMn_2H_{4.6}$ respectively. The R factors could be slightly improved by allowing nonequivalent values of magnetic moments on the Mn(1) and Mn(2) sites and by allowing an arbitrary rotation between the magnetic moments lying in neighboring ab planes ($\neq 2\pi/n$). The best fits ($R_{mag} = 10\%$, 14% , and 17% for $(Lu_{0.4}Y_{0.6})Mn_2H_{4.6}$, $ErMn_2H_{4.6}$, and $TmMn_2H_{4.6}$, respectively) were obtained for a model assuming nonmagnetic Mn(1) sites and an angular shift $\alpha_{1,2}$ between the neighboring *kagomé* planes equal to 130° and 230° ($\alpha_1 + \alpha_2 = 360^\circ$). Although the later model provides slightly lower R factors, the “incommensurate” angular shifts between the *kagomé* planes is difficult to explain from

a physical point of view. If we assume first-neighbor interactions only, an incommensurate rotation between the neighboring *kagomé* planes should yield an incommensurate spiral magnetic modulation along the c axes, 230° ($\alpha_1 + \alpha_2 \neq 360^\circ$), and additional magnetic peaks on neutron diffraction patterns which were not observed experimentally. Moreover, this model assumes very different magnetic moments on Mn(1) and Mn(2) sites. Notice that when we constrained $\alpha_{1,2}$ to “commensurate” values ($\alpha_{1,2} = 360/n$) and allowed the magnetic moments on the Mn(1) and Mn(2) sites to vary independently we always obtained $\mu_{Mn1} \approx \mu_{Mn2}$. The above ambiguity concerns the magnetic stackings *between* the magnetic planes, but does not concern the magnetic ordering *inside* the *kagomé* planes. The analysis of magnetic ordering inside the *kagomé* planes given in the Discussion could be applied indifferently to the models 1 and 2.

The diffuse magnetic peaks observed in the low-content samples $RMn_2H_{4.2}$ are attributed to magnetic correlations having the same propagation vector $\mathbf{k} = 1/3 \ 1/3 \ 0$, but a very short correlation length ($30\text{--}70 \text{ \AA}$). As for the high-content phases, we did not find any magnetic scattering which could be associated with a ferromagnetic ordering (neither long range nor short range). We observe the onset of magnetic ordering (T_N) in the temperature range $150\text{--}200 \text{ K}$, well below the ordering transition in the hydrogen sublattice ($T_H \approx 300 \text{ K}$). The values of T_N are significantly lower than in the high-content phases ($150\text{--}200 \text{ K}$ compared to 250 K) and (as in high-content phases) do not depend on the substitution in the R sublattice. In contrast with the high-content phases, the rare-earth atoms significantly contribute to the

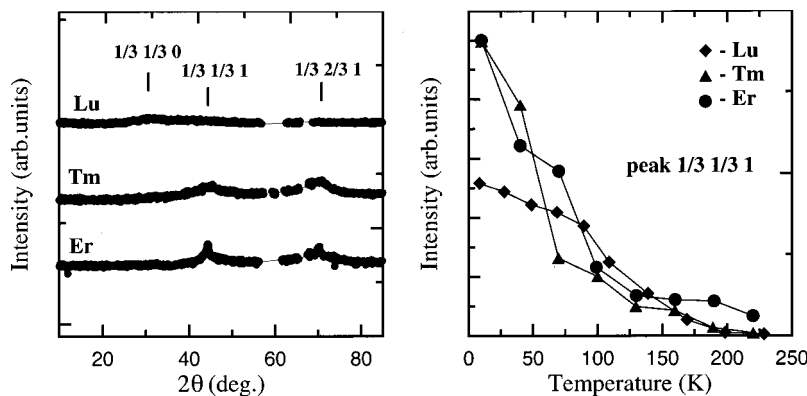


FIG. 4. Left: magnetic scattering in $RMn_2H_{4.2}$ measured on G6.1 ($\lambda = 4.74 \text{ \AA}$) at $T = 10 \text{ K}$. The spectra are subtracted from the neutron diffraction patterns measured in the paramagnetic range ($T = 280\text{--}290 \text{ K}$). Right: integrated intensities of the $1/3 \ 1/3 \ 1$ diffuse peak vs temperature. Solid lines are guides to the eye.

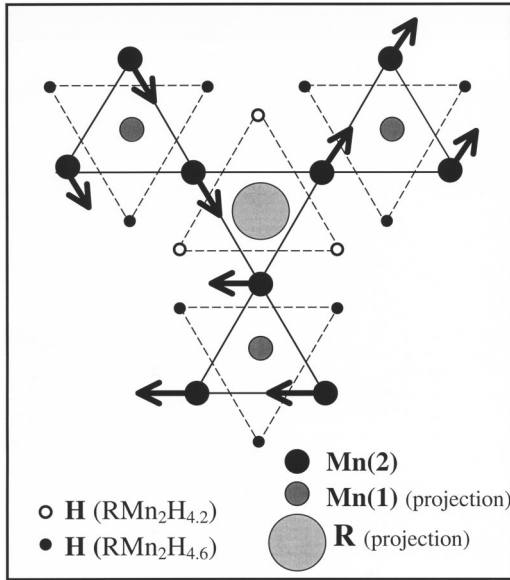


FIG. 5. Hydrogen environments in the high-content and low-content phases and the spin arrangement in the high-content phase inside the Mn(2) *kagomé* planes. Only hydrogen atoms occupying $2R+2Mn$ sites are shown. We also show projections of the rare-earth and Mn(1) atoms lying below and above the *kagomé* planes.

magnetic intensities at the lowest temperatures. Moreover, the nature of the short-range spin correlation significantly changes with rare-earth substitution (Fig. 4). In LuMn₂H_{4,2} the diffuse magnetic peaks are well described by Gaussian-like profiles. In contrast, in TmMn₂H_{4,2} and ErMn₂H_{4,2} we observe Lorentzian-like contributions to the magnetic peaks. These contributions are much sharper than the Gaussian-like peaks observed in the LuMn₂H_{4,2} and become more important at low temperatures $T \ll T_N$. The correlation lengths (estimated from the widths of the diffuse peaks) are significantly higher in compounds with magnetic rare-earth atoms (see Table IV). The relative intensities of the diffuse mag-

netic peaks observed in TmMn₂H_{4,2} and ErMn₂H_{4,2} differ from those measured in LuMn₂H_{4,2}. The $(1/3 \ 1/3 \ 0)$ peak which is very strong in the LuMn₂H_{4,2} does not exist in ErMn₂H_{4,2} in the whole temperature range. In TmMn₂H_{4,2} the $1/3 \ 1/3 \ 0$ reflection has nonzero intensity in the temperature range $70 < T < 200$ K, but does not exist in the temperature range $T < 70$ K. The variation of the magnetic intensities could be assigned to a reorientation of the rare-earth and Mn moments (while keeping the same propagation vector of the magnetic modulation) induced by the magnetic anisotropy of rare-earth ions, as previously observed in the cubic hydrides RMn₂H_{4,5}.^{13,18}

V. DISCUSSION

The results show that interstitial hydrogen drastically influences the magnetic properties of the hexagonal Laves compounds RMn₂ ($R = \text{Er, Tm, Lu}$). First of all, hydrogen induces localized magnetic moments on the Mn sites by expanding the lattice. In the hydrides with hydrogen content $x = 4.2$ and 4.6 the first-neighbor Mn-Mn distances ($d = 2.9$ and 3.1 Å, respectively) are much larger than in the non-doped compounds ($d = 2.6$ Å) and significantly larger than the critical value $d_c = 2.68$ Å. Ordering temperatures in hydrides are much higher than in the parent compounds and do not depend on the rare earth. We conclude that in the hydrides the Mn magnetism dominates and imposes magnetic ordering on the rare-earth sublattice as in the cubic hydrides. The magnetic properties of hexagonal Laves hydrides could be compared with the magnetic properties of the Laves compounds formed by light rare-earth or $5f$ elements ($R = \text{Pr, Nd, Th}$) having larger ionic radii and localized Mn moments.

There is an important difference between the cubic and hexagonal Laves hydrides RMn₂H_{4+x}. In the cubic hydrides RMn₂H_{4,5} the magnetic and hydrogen sublattices order simultaneously through a first-order magnetostructural transi-

TABLE III. Magnetic structure parameters of ErMn₂D_{4,6} at $T = 10$ K. Propagation vector $\mathbf{k} = 1/3 \ 1/3 \ 0$.

Atom	x	y	z	Model 1			Model 2		
				$\mu_x(\mu_B)$	$\mu_y(\mu_B)$	$\mu_z(\mu_B)$	$\mu_x(\mu_B)$	$\mu_y(\mu_B)$	$\mu_z(\mu_B)$
Er(1)	0.333	0.667	0.059	-2.5(6)	0.00	0.00	-2.9(2)	0.00	0.00
Er(2)	0.333	0.667	0.441	2.5(6)	2.5(6)	0.00	2.9(2)	2.9(2)	0.00
Er(3)	0.667	0.333	-0.059	0.00	-2.5(6)	0.00	0.000	-2.9(2)	0.00
Er(4)	0.667	0.333	0.559	-2.5(6)	0.0	0.00	-2.9(2)	0.00	0.00
Mn(1-1)	0.000	0.000	0.000	1.5(1)	3.0(2)	0.00	0.000	0.00	0.00
Mn(1-2)	0.000	0.000	0.500	1.5(1)	3.0(2)	0.00	0.000	0.00	0.00
Mn(2-1,2,3)	-0.158	-0.317	0.250	2.6(2)	0.000	0.00	2.7(2)	0.00	0.00
	0.317	0.158	0.250						
	-0.158	0.158	0.250						
Mn(2-4,5,6)	-0.317	-0.158	-0.250	-2.6(2)	0.000	0.00	-0.5(3)	2.4(1)	0.00
	0.158	0.317	-0.250						
	0.158	-0.158	-0.250						
Reliability factor				$R_m = 20\%$			$R_m = 14\%$		

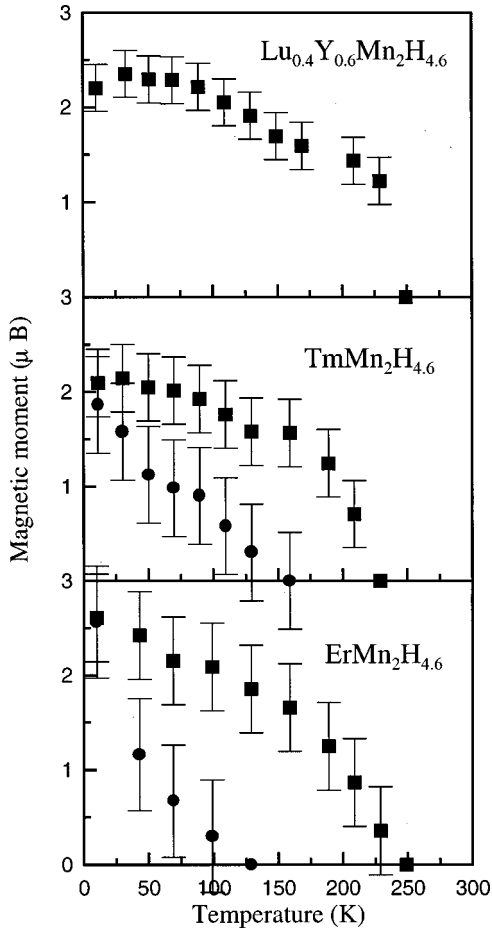


FIG. 6. Temperatures dependences of the Mn and rare-earth magnetic moments (■ and ●, respectively) in the $RMn_2H_{4.6}$ compounds.

tion. In the hexagonal compounds the two sublattices order at different temperatures by second-order-like transitions. These phenomena could be well explained in the frame of the model proposed in Ref. 13. One can calculate a mean-field exchange energy E^{MF} in the ordered hydride and the corresponding characteristic temperature $(3/2)kT^{MF} = E^{MF}$. If we assume that hydrogen atoms are always ordered, T^{MF} will be equal to the experimentally measured Néel temperature T_N . In reality, in the cubic hydrides T^{MF} is higher than the hydrogen ordering temperature T_H . As shown in Ref. 19, hydrogen disorder suppresses magnetic long-range ordering. Therefore no long-range magnetic ordering is expected in the temperature range $T > T_H$. Consequently, T^{MF} corresponds only to a “virtual” Néel temperature and the magnetic ordering occurs at T_H together with the hydrogen ordering. In the

TABLE IV. Spin correlation lengths in the $RMn_2H_{4.2}$ compounds.

Compounds	Peak shape	Correlation lengths (Å)
$LuMn_2H_{4.2}$	Gaussian	32
$TmMn_2H_{4.1}$	Lorentzian	38
$ErMn_2H_{4.2}$	Lorentzian	73

hexagonal hydrides, the magnetic energy is lower (because of shorter Mn-Mn distances and weaker Mn moments) and $T^{MF} < T_H$. Therefore magnetic and hydrogen orderings occur at different temperatures $T_N = T^{MF}$ and T_H , respectively.

The most surprising and interesting feature is the very high sensitivity of the magnetic ordering to small variations of hydrogen content and to particular types of hydrogen superstructure. The strong coupling between the hydrogen superstructure and the magnetic ordering has been already observed in the cubic hydrides $RMn_2H_{4.5}$.^{12,13,19} It was found that hydrogen disorder (induced by chemical doping in the Mn sublattice) destroys long-range magnetic ordering and stabilizes short-range magnetic correlations. Here we observe a breakdown of long-range magnetic ordering induced by a structural transition which is not associated with a chemical disorder. The simple transition from one ordered hydrogen superstructure to another one suppresses long-range magnetic ordering.

We analyze the coupling of magnetic and structural orderings within the model proposed in Ref. 13. This model assumes that the value (and possibly the sign) of the first-neighbor Mn-Mn exchange interaction (J_{Mn-Mn}) depends on the local hydrogen environment. By making J_{Mn-Mn} interactions nonequivalent, hydrogen ordering releases the topological frustration and induces long-range magnetic ordering in the Mn sublattice. In the hexagonal compounds, the hydrogen atoms fill some of the $2R + 2Mn$ interstitial sites in the *kagomé* planes and form “hydrogen triangles” coupled to “Mn triangles” (Fig. 5). Some of the Mn triangles are surrounded by hydrogen atoms, whereas others are not. In the high-content ($x = 4.6$) phase the “H-surrounded” and “H-nonsurrounded” Mn triangles correspond to ferromagnetic and antiferromagnetic triangles in the magnetic structure, so the symmetries of the magnetic and structural orderings inside the *kagomé* planes coincide. The ferromagnetic triangles belong to the Mn(2)-Mn(1) chains which develop along the *c* axes and mediate the interplane magnetic exchange between the Mn(2) planes through the first-neighbor Mn(2)-Mn(1) interactions. Therefore the intraplane magnetic ordering can transform to a three-dimensional magnetic structure. Because the rare-earth atoms are located at the centers of the antiferromagnetic triangles, the mean field of the Mn sublattice on the rare-earth sites should be equal to zero (if we assume first-neighbor interactions only). It explains the strong reduction of the ordered magnetic moments on the rare-earth sites.

Because of the short-range nature of the magnetic correlation in the low-content phases, we cannot prove a precise model for the spin arrangements in the $RMn_2H_{4.2}$ samples. Only the propagation vector and correlation length could be determined unambiguously from our diffraction data. Nevertheless, our structural data show an important difference between “low-content” and “high-content” hydrogen superstructures, which could be responsible for the breakdown of the long-range magnetic ordering. The ways how the H triangles (lying in the *kagomé* planes) surround the Mn triangles are different in the $x = 4.2$ and 4.6 phases. In the low-content samples the hydrogen triangles surround the Mn triangles which form the Mn(2)-*R* interplane chains, whereas the Mn(2)-Mn(1) chains have no hydrogen neigh-

bors in the *kagomé* planes: i.e., the Mn-H coupling is exactly opposite to that found in the high-content samples. Therefore we might expect opposite effects of the hydrogen ordering on the magnetic properties of the low-content phases: namely, a nonzero exchange field on the rare earths, but a reduced magnetic exchange along the Mn(2)-Mn(1) chains. A nonzero exchange field on the *R* sites could explain the larger values of the ordered rare-earth moments (compared to the $x=4.6$ samples), whereas the suppression of the magnetic ordering along the Mn(2)-Mn(1) chains could be responsible for the breakdown of the long-range magnetic ordering.

In the above models we considered the coupling of magnetic and hydrogen ordering inside the *kagomé ab* planes. It is less obvious to explain the influence of hydrogen atoms lying *out* of the *kagomé* planes on the magnetic interactions between the Mn(1) and Mn(2) planes. For the high-content samples (model 1: see Table III), the relative orientations of the magnetic moments in the neighboring *ab* planes are either parallel or antiparallel. Parallel and antiparallel orientations alternate along the *c* axis: therefore, the magnetic surrounding of each Mn plane is nonsymmetric with respect to the *c* axis, whereas hydrogen surroundings are always symmetric. This disagreement could be attributed to the restrictions of the above model which takes into account the first-neighbor Mn-Mn interactions and the first-neighbor Mn-H surroundings only. We note that the second-neighbor magnetic exchange could play a role for interplane magnetic interactions in the hexagonal Laves compounds. In particular, an antiferromagnetic coupling (similar to that found in the

hydrides) between *kagomé* planes had been found in ThMn_2 .⁸ In ThMn_2 the Mn(1) atoms are believed to be nonmagnetic, so that the interplane magnetic interactions cannot be mediated by the first-neighbor exchange in this sample.

In conclusion, our data show the very strong sensitivity of magnetic ordering to very small modifications of hydrogen superstructures. Some of these features could be understood by a model taking into account the local influence of hydrogen atoms on the Mn-Mn exchange interactions. The above model is still obviously oversimplified as it takes into account first-neighbor interactions only and fully ignores the influence of hydrogen superstructures on the band structure. The high-content hexagonal hydrides bring another interesting feature which was not considered up to now. Filling the $2R+3Mn$ interstitial sites could influence the magnetic properties of both Mn and rare-earth sublattices. In particular, hydrogen located in the $2R+3Mn$ sites could contribute to the strong suppression of the rare-earth magnetic moments in the high-content samples.

Ab initio calculations of influence of the hydrogen superstructures on the band structure and experimental study of an interplay of magnetic and hydrogen ordering in the hydrides having lower hydrogen contents $0 < x < 4$ (now in progress) could help in a further understanding of the problem.

ACKNOWLEDGMENTS

This work was partly supported by the Russian foundation for Basic Research, Grant No. 02-02-06085, and the Russian State Program "Neutron Investigations of Condensed Matter."

*Corresponding author. FAX: 33-1-69-08-82-61. Electronic address: gonch@llb.saclay.cea.fr

¹G. P. Felcher, L. M. Corliss, and J. M. Hastings, *J. Appl. Phys.* **36**, 1001 (1965).

²B. Ouladdiaf, R. Ballou, J. Deportes, R. Lemaire, and F. Sayetat, *J. Phys.: Condens. Matter* **4**, 4675 (1992).

³I. Yu. Gaidukova, S. B. Kruglyashev, A. S. Markosyan, R. Z. Levitin, Yu. G. Pastushenkov, and V. V. Snegirev, *Sov. Phys. JETP* **57**, 1083 (1983).

⁴C. Ritter, S. H. Kilcoyne, and R. Cywinski, *J. Phys.: Condens. Matter* **3**, 727 (1991); **4**, 1559 (1992).

⁵B. Ouladdiaf, C. Ritter, R. Ballou, and J. Deportes, *Physica B* **276-278**, 670 (2000).

⁶R. Cywinski, S. H. Kilcoyne, and C. A. Scott, *J. Phys.: Condens. Matter* **3**, 6473 (1991).

⁷I. Yu. Gaidukova and A. S. Markosyan, *Phys. Met. Metallogr.* **54**, 168 (1982).

⁸J. Deportes, R. Lemaire, B. Ouladdiaf, E. Roudaut, and F. Sayetat, *J. Magn. Magn. Mater.* **70**, 191 (1987).

⁹M. Latroche, V. Paul-Boncour, J. Przewoznik, A. Percheron-

Guégan, and F. Bourée-Vigneron, *J. Alloys Compd.* **231**, 99 (1995).

¹⁰J. Przewoznik, J. Zukrowski, and K. Krop, *J. Magn. Magn. Mater.* **187**, 337 (1998).

¹¹J. Przewoznik, J. Zukrowski, K. Freindl, E. Japa, and K. Krop, *J. Alloys Compd.* **284**, 31 (1999).

¹²I. N. Goncharenko, I. Mirebeau, A. V. Irodova, and E. Suard, *Phys. Rev. B* **56**, 2580 (1997).

¹³I. N. Goncharenko, I. Mirebeau, A. V. Irodova, and E. Suard, *Phys. Rev. B* **59**, 9324 (1999).

¹⁴P. J. Viccaro, G. K. Shenoy, D. Niarchos, and B. D. Dunlap, *J. Less-Common Met.* **73**, 265 (1980).

¹⁵K. H. J. Bushow and R. C. Sherwood, *J. Appl. Phys.* **48**, 4643 (1977).

¹⁶J. Rodriguez-Carvajal, *Physica B* **192**, 55 (1993).

¹⁷A. C. Switendick, *Adv. Chem. Phys.* **167**, 281 (1978).

¹⁸P. Cadavez-Peres, I. N. Goncharenko, and I. Mirebeau, *Phys. Rev. B* **64**, 094419 (2001).

¹⁹I. Mirebeau, I. N. Goncharenko, D. Andreani, and E. Suard, *Phys. Rev. B* **62**, 9493 (2000).